AGU PUBLICATIONS

JGR

Journal of Geophysical Research: Atmospheres

RESEARCH ARTICLE
10.1002/2013JD020159

**Special Section:**
Study of Houston Atmospheric Radical Precursors (SHARP)

**Key Points:**
- Total HCHO emissions are measured from industrial sources in Houston
- Industrial HCHO emission plumes are photochemically modeled
- Primary emissions generally dominate HCHO emissions on local spatial scales

**Correspondence to:**
J. K. E. Johansson,
john.johansson@chalmers.se

**Citation:**
Johansson, J. K. E., J. Mellqvist, J. Samuelsson, B. Offerle, J. Moldanova, B. Rappenglück, B. Lefer, and J. Flynn (2014), Quantitative measurements and modeling of industrial formaldehyde emissions in the Greater Houston area during campaigns in 2009 and 2011, *J. Geophys. Res. Atmos.*, *119*, 4303–4322, doi:10.1002/2013JD020159.

Received 6 MAY 2013
Accepted 6 FEB 2014
Accepted article online 11 FEB 2014
Published online 9 APR 2014

# Quantitative measurements and modeling of industrial formaldehyde emissions in the Greater Houston area during campaigns in 2009 and 2011

**John K. E. Johansson[1], Johan Mellqvist[1], Jerker Samuelsson[1], Brian Offerle[1], Jana Moldanova[2], Bernhard Rappenglück[3], Barry Lefer[3], and James Flynn[3]**

[1]Department of Earth and Space Sciences, Chalmers University of Technology, Gothenburg, Sweden, [2]IVL Swedish Environmental Research Institute, Gothenburg, Sweden, [3]Department of Earth and Atmospheric Sciences, University of Houston, Houston, Texas, USA

**Abstract** A sensitive Mobile differential optical absorption spectroscopy (DOAS) system with real-time evaluation capability and HCHO detection limit of 3 ppb over 100 m has been developed. The system was operated together with a Solar Occultation Flux system for large-scale vertical flux measurements of HCHO, $NO_2$, $SO_2$, and VOCs in the Houston-Galveston-Brazoria area during two studies, in 2009 (Study of Houston Atmospheric Radical Precursors campaign) and in 2011 (Air Quality Research Program study). Both in 2009 and 2011, HCHO plumes from five separate local sources in Texas City, Mont Belvieu, and Houston Ship Channel (HSC) were repeatedly detected using Mobile DOAS with emissions varying between 6 and 40 kg/h. In many cases significant alkene emissions were detected simultaneously with the HCHO plumes. Furthermore, in 2011 two additional sources were observed in Texas City and in HSC, with 10 kg/h and 31 kg/h HCHO, respectively. A plume chemistry model was applied to 13 cases to investigate whether the detected HCHO was emitted directly from the industries or was produced by photochemical degradation of VOCs. The model results showed that on average 90% of the detected HCHO was of primary origin and the photochemical production contributed more than 10% in only three cases. Based on the repeatability, it is likely that the most significant HCHO sources in the area are included in this study with an overall emission of 120 kg/h. On a regional scale, this emission is small compared to the secondary HCHO formed from oxidation of reactive VOCs emitted from the same industries, estimated to be an order of magnitude higher.

## 1. Introduction

Houston, Texas, is the largest city in Texas and the fourth largest city in the United States. The Houston-Galveston-Brazoria area (HGB), encompassing the counties of Brazoria, Chambers, Fort Bend, Galveston, Harris, Liberty, Montgomery, and Waller, was designated a nonattainment area for the National Ambient Air Quality Standards for ozone in 2004. The 8 h ozone standard, defined as the *annual fourth highest daily maximum 8 h concentration*, *averaged over 3 years*, had been set at a level of 80 ppbv in 1997 (changed to 75 ppbv in 2008).

Ground level ozone is primarily formed through photochemical smog, a tropospheric process fueled by nitrogen oxides ($NO_x$), volatile organic compounds (VOC), and solar radiation. Key factors affecting ground ozone levels are thus not only local emissions of $NO_x$ and VOC and local solar radiation but also regional emissions and metrological conditions responsible for dilution and transport. In urban settings, $NO_x$ and VOC emissions are typically dominated by anthropogenic sources, primarily from motor vehicular transport and heavy industry; however, biogenic sources of VOC can also be important in rural areas. Unique for the HGB area compared to other urban areas is its heavy concentration of refineries and petrochemical industries, associated primarily with large VOC emissions but also with significant $NO_x$ emissions.

Two large measurement campaigns undertaken in the HGB area, TexAQS (Texas Air Quality Study) in 2000 and TexAQS II in 2006, aimed to quantify emissions and to explain the causes of ozone exceedance events. Several studies based on measurements from these campaigns showed that existing emission inventories severely underestimated VOC emissions in the area, often by up to an order of magnitude [*Kleinman et al.*, 2002; *Karl et al.*, 2003; *Ryerson et al.*, 2003; *Wert et al.*, 2003; *Jobson et al.*, 2004; *De Gouw et al.*, 2009; *Parrish et al.*, 2009;

*Mellqvist et al*., 2010; *Washenfelder et al*., 2010]. The contribution of different VOCs to total OH reactivity was studied with ground-based [*Jobson et al*., 2004], ship-based [*Gilman et al*., 2009], and aircraft-based measurements [*Washenfelder et al*., 2010], since this is an indicator of importance of the individual VOCs for ozone formation, at least in the short term. Although the results differed slightly, the total OH reactivity was mainly dominated by ethene, propene, formaldehyde, and acetaldehyde in relatively fresh industrial plumes from Houston Ship Channel (HSC), the largest conglomerate of petrochemical industries in the HGB area. Since acetaldehyde is formed as a secondary product through oxidation of propene and formaldehyde is formed through oxidation of both ethene and propene, ethene and propene might alone be responsible for most of the short-term ozone formation from industrial VOC emissions in HGB. This notion is supported by the conclusion by *Wert et al*. [2003] and *Parrish et al*. [2012] that formaldehyde and acetaldehyde in HGB industrial emission plumes are mainly of secondary origin. However, three studies based on statistical correlation of formaldehyde in ambient air with other species [*Friedfeld et al*., 2002; *Rappenglück et al*., 2010; *Buzcu Guven and Olaguer*, 2011] attributed a significant part to primary industrial sources.

Primary formaldehyde is known to be formed through incomplete combustion, such as in industrial flares, but since this formation is poorly understood, formaldehyde emissions from combustion are typically not included in industrial emission inventories. If significant primary industrial sources of formaldehyde exist, they might play a key role in ozone production since they may accumulate overnight and kick-start smog formation in the morning through photolysis of HCHO into $HO_2$ [*Parrish et al*., 2012]. Secondary formaldehyde could not play this role since it is a product of the smog it would supposedly kick-start.

During the 2009 Study of Houston Atmospheric Radical Precursors (SHARP) campaign several complementary studies focused on the same industries in Texas City and Mont Belvieu. Concentration measurement by the Aerodyne mobile lab [*Kolb et al*., 2004; *Wood et al*., 2012] showed formaldehyde emissions from two different flares, one in Texas City and one in Mont Belvieu. Based on measurements of ratios of HCHO to CO by Aerodyne mobile lab and inverse modeling, *Olaguer et al*. [2013] have derived significant emissions from an area with several large flares in Texas City. Using Multi-Axis differential optical absorption spectroscopy (DOAS), *Stutz et al*. [2011] estimated significant emissions of formaldehyde from the Texas City facility, correlating with $SO_2$. Formaldehyde emissions were also detected right at the tip of flares in Texas City, Mont Belvieu, and HSC using Imaging DOAS [*Pikelnaya et al*., 2013], conclusively pinpointing flares as primary HCHO sources. The objective of this work has been to survey the general emissions of HCHO from oil-related industries using measurements based on optical remote sensing and to investigate whether the HCHO measured was emitted directly at the industries (primary emissions) or produced by photochemical degradation of VOCs (secondary emissions). This was achieved using a plume chemistry model applied to plume measurement data from the two applied optical techniques, in situ data from the nearby Moody Tower and meteorological data as measured by GPS soundings.

## 2. Methods

### 2.1. Flux Measurements

The main measurements in this study were made using Mobile DOAS and Solar Occultation Flux, which are both based on the same principle for flux measurements. The mass flux $\dot{m}$ of a species through a surface $S$ can be written as a surface integral

$$\dot{m} = \iint_S \rho(\mathbf{v}\cdot\mathbf{n})\mathrm{d}A \tag{1}$$

where $\rho$ is the mass density of the species, $\mathbf{v}$ is the wind velocity vector, $dA$ is the differential surface area, and $\mathbf{n}$ is the normalized vector normal to that surface. Mobile DOAS and SOF take advantage of the fact that open path absorption spectroscopy measures column concentrations, which are path integrals of concentrations along the light path. This conveniently takes care of the integration in one dimension and makes it possible to calculate a mass flux through a large surface, such as a downwind cross section of a dispersed plume, simply by making repeated measurements while traversing the surface in the second dimension. Mobile DOAS is based on absorption spectroscopy of UV/visible light scattered in the zenith direction by the atmosphere. Using the relation between mass density and number density, $\rho = Mn/N_a$, where $M$ is the molar mass of the species, $n$ is the number density, and $N_a$ is the Avogadro constant, and assuming that the wind does not vary

with height, we can, for the surface formed by the Mobile DOAS measured light path as it is moved through a plume, write (1) as

$$\dot{m} = \frac{M}{N_a}\int_0^D \left[\int_0^L n(l)\mathrm{d}l\right] v\cos(\alpha)\mathrm{d}x \tag{2}$$

where the inner integral is along the light path, the outer integral is along the path driven by the measurement vehicle, $v$ is the wind speed, and $\alpha$ is the angle between the wind direction and the normal to the path driven. Recognizing the inner integral as an integrated concentration column $C$, which is the result of the spectral retrieval of a Mobile DOAS spectrum, we can approximate (2) as a sum over the series of measurements made while traversing the plume

$$\dot{m} = \frac{M}{N_a}\sum_j C_j v_j \cos(\alpha_j)\Delta x_j \tag{3}$$

where index $j$ denotes a spectrum measurement in the measurement series and $\Delta x_j$ is the distance traveled during that measurement. The spectral evaluation gives $C_j$, the GPS positions recorded throughout the measurements give $\Delta x_j$, and $v_j$ and $\alpha_j$ are obtained through some sort of wind measurement. Variations in wind with time and along the measurement path can be directly applied in (3), but vertical wind variations are trickier. Preferably, the wind velocity used for flux calculations should be the average velocity of the gas measured. However, the spectral measurements give no information about the vertical distribution of the gas and at most times no measurements of vertical wind profiles are available. For this reason, wind uncertainty is estimated to be the largest error source in this type of flux measurements.

### 2.2. Mobile DOAS

Differential optical absorption spectroscopy (DOAS) is a well-established spectroscopic method for measurements of gaseous molecular species using light in the ultraviolet and visible regions [*Platt and Stutz*, 2008]. Mobile DOAS is the application of passive DOAS measurements of atmospherically scattered sunlight for flux measurement as described in the previous section. It has previously been applied for measurements of volcanic emissions of $SO_2$ [*Galle et al*., 2002], industrial emissions of $SO_2$, $NO_2$, and HCHO [*Rivera et al*., 2009, 2010], and $SO_2$, $NO_2$, and HCHO emissions from entire cities and megacities [*Johansson et al*., 2008, 2009; *Ibrahim et al*., 2010; *Wagner et al*., 2010; *Shaiganfar et al*., 2011].

Although HCHO has been measured before with Mobile DOAS, this has generally been measurements of large-scale plumes from entire cities or industrial areas. The objective for the SHARP campaign was to develop a Mobile DOAS system that could measure on the scale of individual point sources with relatively small HCHO emissions but still have the speed and mobility to cover large industrial areas in reasonable time. For this purpose, it was important to have a high throughput of light to the spectrometer to maintain a high signal-to-noise ratio. This was achieved by using a 3 mm thick liquid light guide and a 300 μm wide entrance slit. A relatively high spectral resolution (0.63 nm) was still achieved by only measuring a narrow-wavelength region, 309–351 nm, where HCHO has its largest absorption features. The spectrometer used was a 303 mm focal length Czerny-Turner spectrometer (Andor Shamrock 303i) with a thermoelectrically cooled 1024 × 255 pixel CCD (Charge-Coupled Device) detector (Newton DU920N-BU2) and a holographic grating with 1800 grooves/mm. The spectrometer was connected with the liquid light guide to a zenith-looking quartz telescope with a 75 mm diameter and a 20 mrad (1.15°) field of view. The telescope was equipped with an optical band-pass filter (Hoya), blocking wavelengths above 380 nm to reduce stray light in the spectrometer. Wavelength calibration and instrument line shape was obtained by regular measurements of the spectrum from a low-pressure mercury-vapor lamp.

HCHO and $NO_2$ were evaluated in the wavelength region 324–350 nm. To achieve the low detection limit made possible with high throughput of light it was also important to have a carefully calibrated instrument and a retrieval algorithm capable of handling some common error sources. The wavelength calibration was improved for each measurement series separately by correlation of the Fraunhofer lines in the reference spectrum to those in a high-resolution solar spectrum [*Kurucz*, 1994]. The cross sections were degraded to the resolution of the spectrometer using the instrument line shape measured with a mercury lamp and sampled with the wavelength calibration of the reference spectrum to ensure that the reference and the cross sections would be on the same absolute wavelength scale. Due to this, only 1° of freedom for wavelength shifting, that of the evaluated spectrum

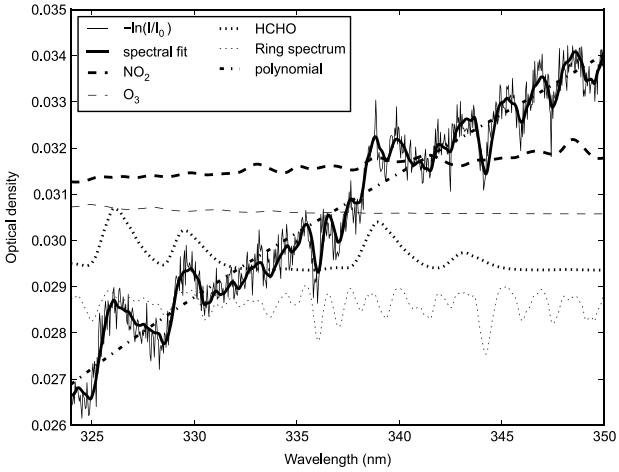


**Figure 1.** DOAS spectral fit for a spectrum measured inside a plume. The different components of the fit, $NO_2$, $O_3$, HCHO, Ring spectrum, and polynomial, are also shown. All components except the polynomial have been shifted in *y* direction for illustrative purpose.

caused by vibrations and temperature variations, needed to be included in the spectral fitting routine. The spectral evaluation included cross sections of HCHO [*Cantrell et al.*, 1990], $NO_2$ [*Vandaele et al.*, 1998], $O_3$ [*Burrows et al.*, 1999], $(O_2)_2$ collision complex [*Hermans et al.*, 1999], a synthetic Ring spectrum to account for the Ring effect caused by inelastic scattering, a polynomial of order 3 to account for broadband spectral effects of scattering, shift, and stretch parameters for the evaluated spectrum to account for small changes in the wavelength calibration during the measurements, and an offset polynomial of order 2 fitted to account for stray light in the spectrometer. Stray light was estimated to be approximately 0.2–0.4% of the true spectral light in the wavelength region used. The spectral fit for a spectrum measured inside a plume is shown in Figure 1. The QDOAS software [*Fayt*, 2011] was used for the wavelength calibration, degradation of cross sections, Ring spectrum synthesis, and spectral fitting. During typical operations in good weather conditions, this Mobile DOAS system was able to make HCHO column retrievals with a $1\sigma$ precision of 0.4 mg/m$^2$, which corresponds to approximately 3 ppbv over a height of 100 m, for a sampling time of 1–2 s. During the 2009 study, measurements were performed offline and all spectral evaluations were made afterward, but for the 2011 study, high-quality real-time evaluation was implemented, providing highly useful feedback to the operators performing the measurements.

In the 2009 study, measurements were carried out from a Volkswagen transporter, while a pickup truck was used in 2011. When performing a Mobile DOAS measurement series a reference spectrum is typically recorded in what is assumed to be clean ambient air. Spectra are then measured repeatedly, while the vehicle is driven along a route chosen to make the DOAS measurement path slice through an industrial emission plume, preferably as perpendicularly as possible to the wind direction. Time and position for each spectrum is simultaneously recorded using a GPS (Global Positioning System) receiver. Figure 2 illustrates the principles for this type of measurement. As shown here, an isolated industrial facility emitting its plume into a fairly homogenous background air mass, will show up in the time series of evaluated column concentrations as a peak on top of a fairly constant baseline. Most industrial areas are, however, a patchwork of many industries, and these time series need to be manually interpreted as plumes from different areas.

### 2.3. SOF Measurements

The Mobile DOAS measurements were performed in parallel with SOF (Solar Occultation Flux) measurements from the same measurement vehicle. The SOF method is presented in detail by *Mellqvist et al.* [2010]. In many aspects SOF and Mobile DOAS are similar. While Mobile DOAS is based on measuring UV spectra of solar light scattered in the atmosphere, SOF is based on measuring IR spectra of direct solar light using an Fourier transform infrared (FTIR) spectrometer. Measuring direct solar light requires a solar tracker, an electronically regulated mechanical device of mirrors, reflecting the solar light in to the spectrometer, regardless of orientation. SOF and Mobile DOAS measurements are complementary, as they can measure distinctly separate sets of species. The SOF-measurable species primarily of interest for this study are hydrocarbons, specifically ethene and propene. Spectral evaluations for SOF are based on the same theory as for Mobile DOAS, although the implementation differs in the details. Flux calculations are also made in the same way, except that the evaluated column concentrations are first multiplied by the factor $\cos\theta$, where $\theta$ is the solar zenith angle (SZA), to compensate for the fact that the measured light does not pass the plume vertically.

For this study a custom built solar tracker was used together with a Bruker IR-cube FTIR-spectrometer with 0.5 cm$^{-1}$ spectral resolution and a combined MCT (Mercury Cadmium Telluride) and InSb (Indium

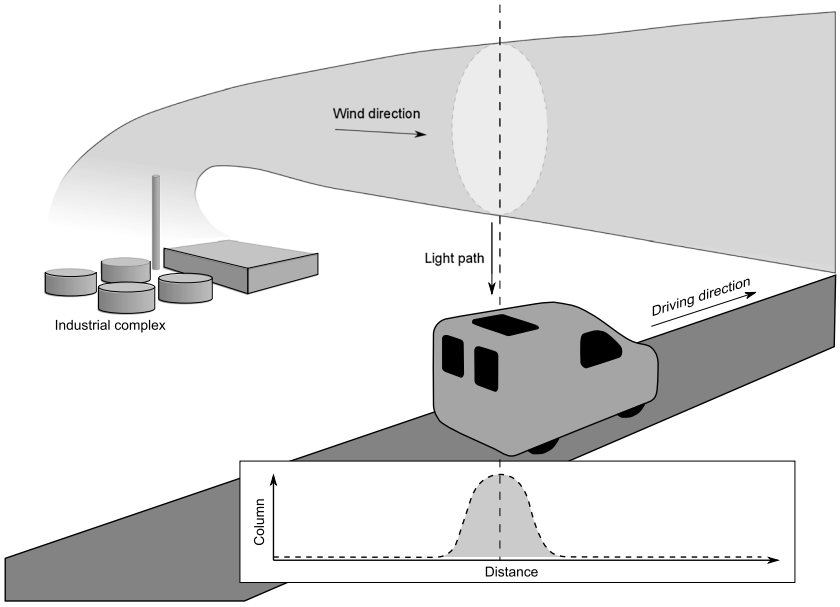


**Figure 2.** Illustration of the principles for Mobile DOAS plume measurements. A plume is traversed as perpendicularly to the wind direction as possible while zenith sky spectra of scattered light are measured continuously. DOAS spectral evaluation of the spectra gives a series of columns for the species of interest, which can be plotted against the distance traveled, showing a profile for the plume. The area under this profile multiplied with the wind speed through the plume cross section gives the flux for the species of interest in the plume.

Antimonide) detector. Ethene and propene were evaluated in the spectral region 900–1000 $cm^{-1}$, where they have strong absorption lines at 949 $cm^{-1}$ and 912 $cm^{-1}$, respectively. The spectral evaluation typically showed an unsystematic $1\sigma$ variation of 0.8 and 1.4 $mg/m^2$ for ethene and propene, respectively. During the measurement campaign, the solar tracker had periods of reduced performance, which resulted in distorted spectra causing reoccurring spikes in the evaluated plume profile. These spikes were sorted out using a threshold for the root-mean-square error of the spectral evaluation.

### 2.4. Wind Measurements

A major concern for flux calculations based on Mobile DOAS and SOF measurements is the occurrence of vertical wind speed gradients. Wind speeds typically increase with height which together with uncertainty in height distribution of the emission plumes gives uncertainties in flux calculations. However, the meteorological conditions needed to make good spectral measurements, clear and sunny skies, fortunately mitigate this problem. Sunny conditions are associated with vertical instability and convection, which causes smoothing of vertical wind gradients as well as faster vertical mixing of emission plumes, both of which decrease the uncertainty of flux calculations.

Doppler lidar measurements during the TexAQS II campaign [*Tucker et al.*, 2009] showed typical daytime vertical mixing speeds of ±(0.5–1.5) m/s, while airborne measurements during the same campaign encountered an alkene plume mixed up to 600 m only 250 s downwind of its source, indicating a vertical mixing speed of almost 2.5 m/s [*Mellqvist et al.*, 2010].

During the SHARP campaign, wind height profiles were regularly measured using GPS-tracking radiosondes launched with helium balloons from three locations in HGB, Lynchburg Ferry in HSC, K Ranch in Mont Belvieu, and the south side of the refinery area in Texas City. These locations are marked LF, MB, and TC, respectively in Figure 3. All together 71 radiosondes were launched on 27 separate days. Average winds for the height interval 0–500 m were calculated from these profiles, since this was considered representative of the vertical distribution of the investigated plumes. The difference in wind speed between 0–500 m averages and, for instance, 0–200 m averages was only a couple of percent on average, which demonstrates the lack of large-vertical wind gradients and the possibility of making relatively robust flux calculations. Since wind profile measurements were not available for all flux calculations, they were supplemented with wind data from

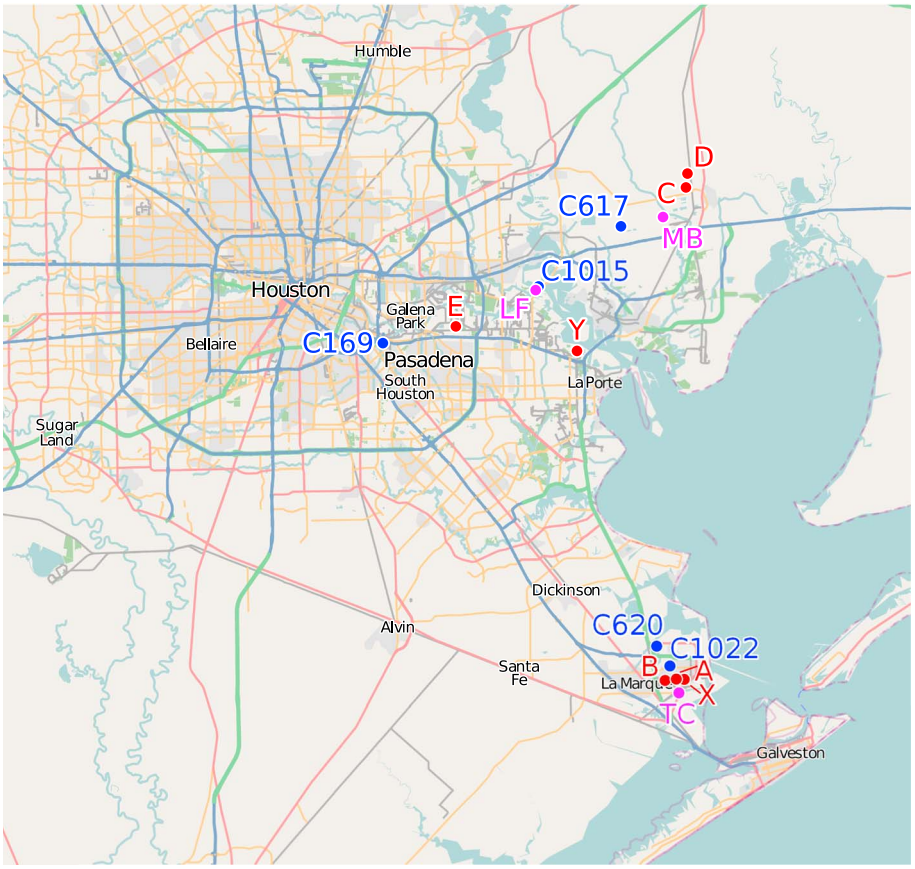


**Figure 3.** Map of Houston and its eastern and southern surroundings. The locations of radiosonde launch sites, ground sites (CAMS) for wind measurements, and the seven formaldehyde sources found are marked in magenta, blue, and red, respectively.

ground-based mast measurements. Wind data from five different CAMS (Continuous Air Monitoring Stations), C1015 by Lynchburg Ferry, C169 in the southwestern part of HSC, C617 between Mont Belvieu and Baytown, C620 and C1022 north of the Texas City industries, were used. The locations of these stations are also marked in Figure 3. Wind speeds measured by ground-based masts are typically lower than radiosonde measurements due to retardation by the ground and its structures. The magnitude of the difference depends on mast height, local topography, buildings, and vegetation. To compensate for the bias of ground level measurements, wind speeds measured by masts were normalized to the 0–500 m sonde averages. This was done by comparing simultaneous measurements and assigning a scaling factor to each mast, making their wind speeds equal to the radiosondes on average. Wind data from C1015 and C169 were compared to radiosondes launched by Lynchburg Ferry (LF), wind data from C617 with sondes launched from Mont Belvieu (MB), and wind data from C620 and C1022 with sondes launched from Texas City (TC). After scaling, the same comparisons were used to estimate the uncertainty of the wind measurements, both in terms of speed and direction. Figure 4 illustrates this comparison for the wind measurements in Texas City as an example. Averages of absolute errors in speed and direction of the CAMS measurements compared to radiosondes are shown in Table 1.

### 2.5. Error Analysis

The main uncertainty for the flux measurements with SOF and Mobile DOAS is due to the uncertainty in the wind field. From the wind speed data in Table 1 the 1$\sigma$ spread relative to the 0–500 m GPS sonde wind is 11–30%. This spread is attributed to the uncertainty in using the 0–500 m wind for the average plume mass transport, which has been used as the most likely plume wind speed during the campaign. The variations among the different ground wind measurements, the 0–100 m, 0–200 m, and 0–500 m averages, for the GPS sondes are assumed to be representative of the variations in wind due to height and spatial location on the

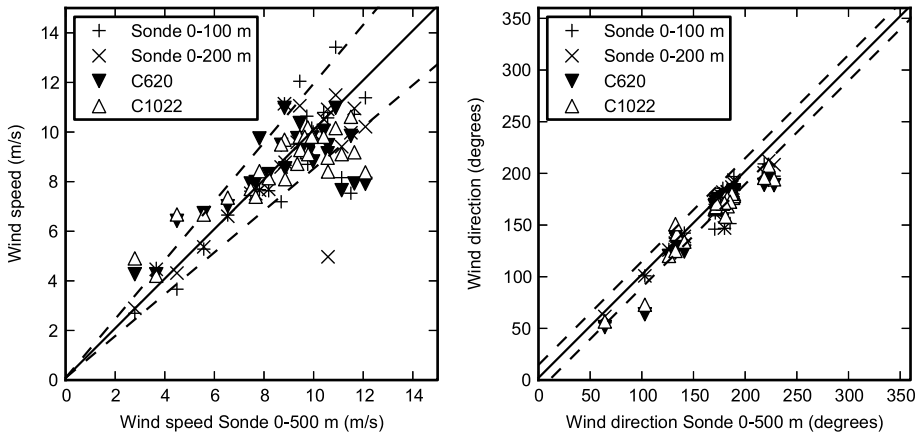


**Figure 4.** Comparison between wind measurements with GPS-tracking radiosondes and scaled CAMS mast measurements in Texas City. Each point compares the 0–500 m wind average measured by a sonde launch on the *x* axis to either the 0–100 m average, the 0–200 m average or to simultaneous ground measurements at C620 or C1022 on the *y* axis. The left plot compares wind speeds, and the right plot compares wind directions. Dashed lines mark the root-mean-square error for all the points in each plot, in relative terms for the wind speed and in absolute terms for the wind direction. Wind speeds measured on the ground have been scaled to remove systematic bias compared to 0–500 m sonde averages.

relevant scales. The impact of the wind direction uncertainty on the flux uncertainty is dependent on how orthogonally the plume is traversed. For orthogonal transects the flux uncertainty is weakly affected by the wind direction uncertainty, while more oblique transect angles introduce a larger uncertainty. The wind direction uncertainty ($1\sigma$) was estimated to be 11–17°, which at the higher end would imply a 5% flux uncertainty for an orthogonal plume transect, and 12% on average for a transect angle of 75°.

In order to estimate the systematic uncertainty in the HCHO column retrieval, three formaldehyde plumes from the 2011 measurements were reevaluated with a number of variations on the spectral retrieval described in section 2.2. Figure 5a shows the HCHO column time series for one of these plumes from the reference retrieval as well as from retrievals using alternative cross sections for the absorbing species. The HCHO cross section from *Cantrell et al*. [1990] was substituted for the corresponding from *Meller and Moortgat* [2000], the $O_3$ cross sections from *Burrows et al*. [1999] were substituted for the corresponding from *Bogumil et al*. [2003], and the $NO_2$ cross section from *Vandaele et al*. [1998] was substituted for the corresponding from *Burrows et al*. [1998]. The $(O_2)_2$ collision complex was simply excluded and the synthesized Ring spectrum produced by QDOAS [*Fayt*, 2011] was substituted for a slightly different one produced by DOASIS [*Kraus*, 2004]. The latter one is synthesized from the reference spectrum measured by the DOAS instrument, while the former uses a high-resolution solar spectrum [*Kurucz*, 1994]. Figure 5b shows a scatterplot of the HCHO columns from the alternative retrievals against the HCHO columns from the reference retrieval, as well as linear functions fitted for each alternative retrieval. The slopes from these linear regressions were used to estimate the uncertainties of the HCHO retrieval due to uncertainties in the cross sections. In addition to the alternative retrievals shown in Figure 5, a few of the other retrieval parameters, such as polynomial and wavelength range, were also varied and evaluated in the same way. The results for all the alternative retrievals are presented in Table 2. A few of the alternative retrievals tried, the ones with no Ring spectrum, no offset or np wavelength shift fitted, gave significantly worse spectral fits and rather

**Table 1.** Results of Comparing CAMS Wind Measurements to 0–500 m Averages of Radiosonde Wind Profiles[a]

| CAMS | Compared to Sondes Launched at | Scale Factor | Wind Speed Error | Wind Direction Error |
|---|---|---|---|---|
| C1015 | LF | 1.16 | ± 16% | 10 ± 10° |
| C169 | LF | 1.64 | ± 12% | 0 ± 10° |
| C617 | MB | 1.46 | ± 30% | −5 ± 17° |
| C620 | TC | 1.36 | ± 20% | −9 ± 11° |
| C1022 | TC | 1.57 | ± 19% | −9 ± 10° |

[a]For each CAMS used, the table presents the scale factor for the wind speed, the root-mean-square relative wind speed error, and the mean and standard deviation of the wind direction error.

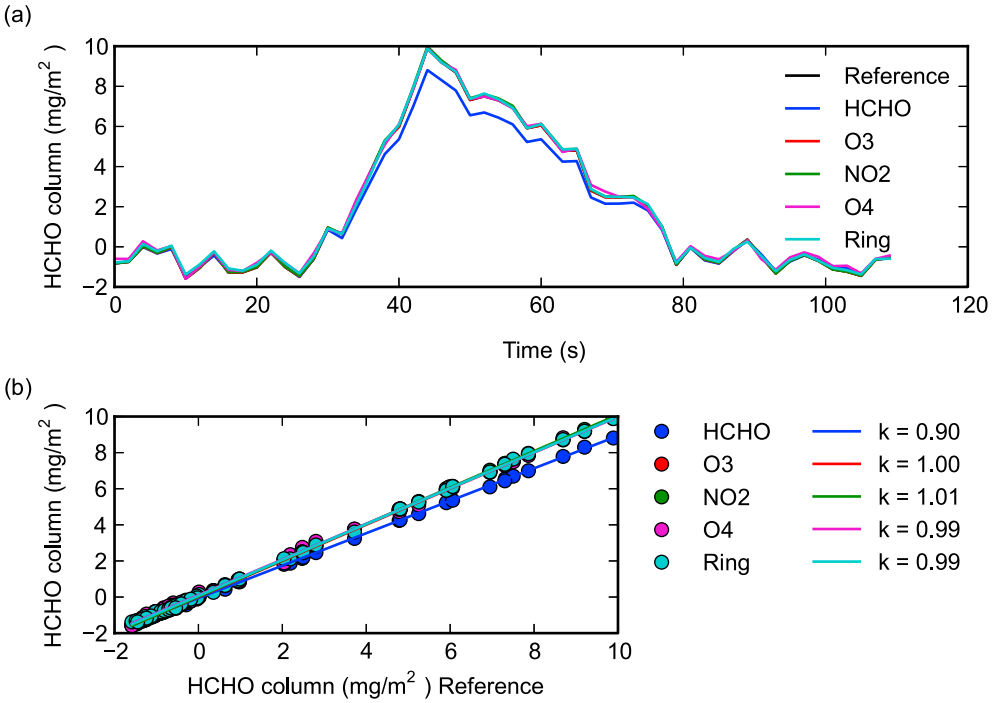


**Figure 5.** (a) HCHO column time series for the reference retrieval of a HCHO plume and variants of this retrieval using alternative cross sections for the different absorbers. (b) Scatterplot of the HCHO columns from the retrieval variants against the corresponding HCHO columns from the reference retrieval together with fitted linear functions with slope *k*.

variable slopes *k*. These retrievals are in italics in Table 2 and were not used to estimate the uncertainty of the retrieval, since they were of lower quality. The retrieval with the HCHO cross section from *Meller and Moortgat* [2000] consistently evaluated 10% lower HCHO columns, which is consistent with the known discrepancy between these two cross sections [*Meller and Moortgat*, 2000]. The other alternative retrievals resulted in no more than a few percent discrepancy. The largest discrepancy for each parameter varied, excluding the lower quality retrievals, was used as an estimate of the uncertainty due to that parameter. These are given in Table 2 (third column). The root-sum-square of all these uncertainties is approximately 11%, which is clearly dominated by the uncertainty of the HCHO cross section.

**Table 2.** Results of Alternative HCHO Column Retrievals for Three Different HCHO Plumes[a]

| Change to Retrieval | *k* | Estimated Uncertainty |
|---|---|---|
| Different HCHO cross section | 0.90 | 10% |
| Different $O_3$ cross section | 1.00 | |
| Different $NO_2$ cross section | 1.01–1.02 | 2% |
| Different Ring spectrum | 0.99–1.02 | 2% |
| *No Ring spectrum* | *0.91–1.01* | |
| No $O_4$ cross section | 0.99–1.00 | 1% |
| Wavelength range 311–336 nm | 0.98–0.99 | |
| Wavelength range 311–350 nm | 0.98–1.01 | 2% |
| Polynomial order 4 | 0.99–1.00 | |
| Polynomial order 5 | 0.98–1.02 | 2% |
| Offset order 1 | 0.98–1.00 | |
| Offset order 0 | 0.97–1.00 | 3% |
| *No offset fitted* | *0.98–1.08* | |
| *No wavelength shift fitted* | *1.02–1.11* | |
| Wavelength shift fitted for reference | 1.00 | |

[a]An interval of slopes from linear regressions of the retrieved columns to the reference retrieval are given. Uncertainty estimates for the reference retrieval based on some of the retrievals are also given. Retrievals in italics were excluded from error estimates due to significantly lower quality of spectral fit.

The uncertainty due to interference from other absorbers is relatively small according to these tests compared to, for instance, MAX-DOAS HCHO measurements [*Pinardi et al.*, 2013]. The primary reason for this is that the magnitude of these absorbers change very little during the measurement of a single-narrow plume, since the measurement elevation angle is constant (zenith) and the plume is generally traversed in less than a minute. With MAX-DOAS, by contrast, measurements are typically performed in multiple elevation angles and over the time scale of a day. This means large changes in for instance $O_3$ and $NO_2$

**Table 3.** Uncertainty Estimation of the Flux Measurements

| | Wind Speed | Wind Direction | Spectroscopy (Cross Sections) | Retrieval Error | Composite Flux Measurement Uncertainty |
|---|---|---|---|---|---|
| Alkanes | 11–30% | 5–12% | 3.5% | 12% | 17–35% |
| Ethene | 11–30% | 5–12% | 10% | 10% | 19–35% |
| Propene | 11–30% | 5–12% | 3.5% | 20% | 24–38% |
| HCHO | 11–30% | 5–12% | 3% | 10% | 16–34% |
| $SO_2$ | 11–30% | 5–12% | 2.8% | 10% | 16–34% |
| $NO_2$ | 11–30% | 5–12% | 4% | 10% | 16–34% |

columns always accompany the HCHO columns of interest. For Mobile DOAS plume measurements on the other hand, the differential columns in the plume typically dominate over background effects.

Effects of aerosol scattering in the plumes, such as multiple scattering and scattering into light path, are not likely to be significant since the plumes were of relatively small dimensions, close to ground and not visible to the naked eye. Absence of variations in absolute light intensity and differential $O_4$ column accompanying the formaldehyde plumes supported this conclusion.

Table 3 shows the composite flux measurement uncertainties for the different species measured with Mobile DOAS and SOF. Apart from the wind uncertainties, these include the uncertainties in the laboratory measured absorption cross sections and retrieval uncertainties estimated to 10–20%. The retrieval uncertainties are dominated by the uncertainty of the plume baseline.

### 2.6. Plume Chemistry Modeling

In order to assess the possibility of formation of secondary formaldehyde in plumes, a photochemical plume model developed at the IVL Swedish Environmental Research Institute and University of Gothenburg was used to simulate the plume chemistry for a number of suitable cases. This model has previously been applied, with small modifications, to chemistry simulations in background air, industrial plumes, shipping plumes, and plumes from traffic emissions and in road tunnel [*Pszenny et al*., 2004; *Svensson et al*., 2004; *Haeger-Eugensson et al*., 2010; *Moldanova*, 2010]. The model is a Lagrangian plume model consisting of two-parallel air parcels, one representing the background air and one representing a continuously expanding plume segment, both moving with a constant wind velocity. The chemical mechanism incorporates gas phase reactions, solar zenith angle dependent photochemical reactions, dry deposition, and background emissions. The photolysis rates, expressed as functions of solar zenith angle, were fitted to values calculated from measured actinic flux data (see section 2.7). In addition to the standard tropospheric $HO_x$, CO, $CH_4$, and $NO_x$ chemistry, the reaction mechanism includes S compounds and nonmethane hydrocarbons. Hydrocarbon chemistry is described with a modified version of the lumped Carbon Bond Mechanism IV (CBM-IV) [*Gery et al*., 1989]. The CBM-IV describes VOC chemistry using eight substance groups, (alkanes, ethene, other alkenes, formaldehyde, higher aldehydes, toluene, and xylene) and keeps the basic steps of the degradation chains in a simplified model. In contrast to *Gery et al*. [1989] oxidation of methane is modeled explicitly and formation of methyl and higher organic peroxides is included as well as formation of carboxylic acids. A loss term for sulfate and nitrate on aerosol derived from *Derwent and Jenkin* [1990] is included in a parameterized form.

For each simulation, the background air and the plume parcel were simultaneously initialized with background concentrations of $O_3$, CO, NO, $NO_2$, $NO_y$, OH, $HO_2$, HCHO, HONO, and $C_2$–$C_{11}$ nonmethane volatile organic compounds (NMVOCs) measured at Moody Tower. Simulation was started 1 h ahead of the plume emission and continuous background emissions of CO, NO, $NO_2$, HONO, $SO_2$, and NMVOCs were set to approximately maintain the appropriate background concentrations. After 1 h of simulation, the plume parcel reached the emission point and the emission fluxes of HCHO, ethene, propene, alkanes, $NO_x$, and $SO_2$ measured with Mobile DOAS and SOF were added. The $NO_2$/NO ratio was assumed to be 5% at emission, which is typical for combustion, and the total $NO_x$ emission was iteratively calculated so that the $NO_2$ flux at the measurement point would match the Mobile DOAS result. Measured fluxes of ethene, propene, and alkanes were used as emission rates since only a small fraction would have been degraded on the time scale from emission to measurement. The model was run iteratively to find a primary emission rate of HCHO that would give the right total HCHO flux at the measurement point. For each iteration the primary HCHO

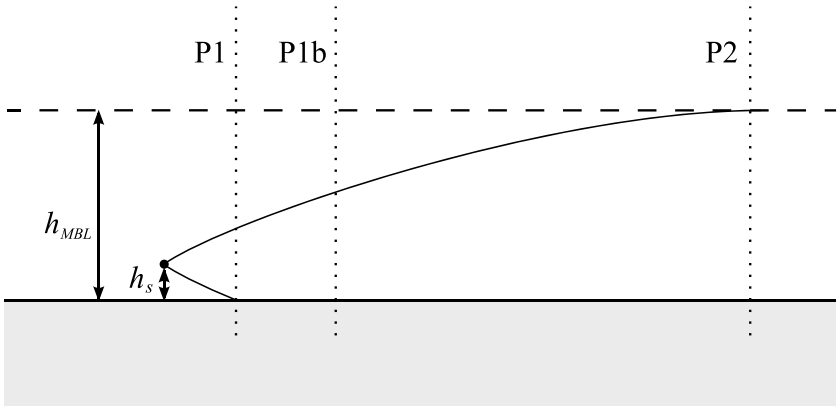


**Figure 6.** Illustration of the plume geometry as modeled in plume chemistry model. The small black circles indicate the plume source, and the dashed line marks the top of the mixing boundary layer. The dotted lines mark the boundaries for the different phases of the plume. The height of the source and the mixing boundary layer are shown as $\boldsymbol{h_s}$ and $\boldsymbol{h_{MBL}}$, respectively.

emission rate was reduced by the difference between simulated and measured HCHO flux at the measurement point in the prior simulation. Since the HCHO production in the model was relatively weakly affected by the primary HCHO, a handful of iterations were generally enough for convergence.

Plume dispersion was modeled as a continuous expansion of the cross-section area of the parcel and a corresponding dilution of the parcel concentration by the background air. The dispersion is described by equations published by *Hanna et al*. [1982].

$$\sigma_y = R_y x^{r_y} \Rightarrow \frac{d\sigma_y}{dx} = r_y R_y x^{r_y - 1} \tag{4}$$

$$\sigma_z = R_z x^{r_z} \Rightarrow \frac{d\sigma_z}{dx} = r_z R_z x^{r_z - 1} \tag{5}$$

where $\sigma_y$ and $\sigma_z$ are dispersion parameters in $y$ (horizontal) and $z$ (vertical) direction, $x$ is distance traveled by the parcel from the source, $R_y$, $r_y$, $R_z$, and $r_z$ are coefficients in the Gaussian plume dispersion correlation. For this model $\sigma_y$ and $\sigma_z$ were taken to be the horizontal and vertical radii of the elliptical cross section of the plume parcel. The dispersion parameters $R$ and $r$ were first set to values for the stability classes [*Klug*, 1969] at the time of the measurements (stability class A or B). $R_y$ and $r_y$ were then modified so the plume width at the point of measurement would be consistent with the one observed in the SOF and Mobile DOAS measurements. The plume geometry as seen from the side is illustrated in Figure 6. The parcel cross-section area was calculated in different ways in three different phases of the plume expansion. In the first phase, from the elevated source until point P1, where the plume reaches the ground, the cross section is a complete ellipse with an area $a$ given by equation (6) and a rate of area increase is given by equation (7).

$$a = \pi \sigma_y \sigma_z = \pi R_y R_z x^{r_y + r_z} \tag{6}$$

$$\frac{da}{dx} = \pi (r_y + r_z) R_y R_z x^{r_y + r_z - 1} \tag{7}$$

In the second phase, from point P1b, where the top of the plume has reached three times the height of the elevated source, to point P2, where the plume reaches the mixing boundary layer height $h_{MBL}$, the cross section is roughly half elliptic with an area given by equation (8) and a rate of area increase is given by (9).

$$a = \frac{\pi}{2} \sigma_y \sigma_z = \pi R_y R_z x^{r_y + r_z} \tag{8}$$

$$\frac{da}{dx} = \frac{\pi}{2} (r_y + r_z) R_y R_z x^{r_y + r_z - 1} \tag{9}$$

In the third phase, from point P2 and beyond, the cross section is roughly rectangular with an area given by equation (10) and a rate of area increase given by (11).

$$a = a_{\mathrm{MBL}} + 2h_{\mathrm{MBL}}\left(\sigma_y - \sigma_{y\mathrm{MBL}}\right) \tag{10}$$

$$\frac{\mathrm{d}a}{\mathrm{d}x} = 2h_{\mathrm{MBL}}\frac{\mathrm{d}\sigma_y}{\mathrm{d}x} = 2h_{\mathrm{MBL}}r_y R_y x^{r_y - 1} \tag{11}$$

where $a_{\mathrm{MBL}}$ and $\sigma_{y\mathrm{MBL}}$ is the cross-section area and horizontal radius at point P2. The cross-section area between point P1 and P1b is given by linear interpolation. The distance of points P1, P1b, and P2 from the source is given by equations (12)–(14)

$$x_{\mathrm{P1}} = \left(\frac{h_s}{R_z}\right)^{\frac{1}{r_z}} \tag{12}$$

$$x_{\mathrm{P1}b} = \left(\frac{2h_s}{R_z}\right)^{\frac{1}{r_z}} \tag{13}$$

$$x_{\mathrm{P2}} = \left(\frac{h_{\mathrm{MBL}} - h_s}{R_z}\right)^{\frac{1}{r_z}} \tag{14}$$

where $h_s$ is the height of the elevated source.

### 2.7. Supplementary Measurements

In addition to the Mobile DOAS and SOF data, supplementary data were needed as input for the plume chemistry model. Background air concentrations and meteorological data were taken from measurements at Moody Tower, located at the campus of University of Houston, about 7 km west of HSC, conducted as a part of the SHARP campaign. This included background concentrations of $O_3$ (measured with UV Photometry), CO (gas filter correlation), NO, $NO_2$, $NO_y$ (Chemiluminescence), $C_2$–$C_{11}$ NMVOC (GC-FID), photolysis rates (calculated from measurements with Scanning Actinic Flux Spectroradiometer, SAFS, and Diode Array Actinic Flux Spectroradiometer, DAFS), boundary layer height (Aerosol Backscatter Ceilometers), temperature, pressure, relative humidity, all measured by University of Houston, as well as HCHO (PTR-MS) measured by Washington State University, OH and $HO_2$ (Ground-based Tropospheric Hydrogen Oxides Sensor-Laser-Induced Fluorescence) measured by Pennsylvania State University, and HONO (Mist Chamber Ion Chromatograph) measured by University of New Hampshire. Details of these measurements can be found in *Lefer* [2009]. Photolysis rates as functions of solar zenith angle were fit to the measured data. One set of functions were fitted to the 50th percentile value for each angle, one to the 70th percentile, and one to the 90th percentile. The 70th percentile functions were used as the default, while the 50th and 90th percentile function were used to test the effects of high and low photolysis rates. The 70th percentile was chosen as default, since the flux measurements were generally made in fairly clear conditions. For a few instances when there were no VOC data available from Moody Tower, auto-GC data from CAMS35, a Texas Commission on Environmental Quality (TCEQ)-operated air quality monitoring site in Deer Park, was used instead. These auto-GC data were also used for speciation of alkanes measured with SOF in the plumes. High-VOC episodes in the auto-GC data, likely to represent fresh plumes from the closest industries, were used for the latter purpose, as opposed to low-VOC episodes used for determination of background levels.

## 3. Results

### 3.1. Formaldehyde Plumes

During the SHARP campaign, the combined SOF/Mobile DOAS platform was in the field from 20 April 2009 until 11 June 2009. In this period, Mobile DOAS measurements were performed on 38 days. The period was, however, dominated by southern-southwestern winds blowing warm, humid air masses in from the Gulf of Mexico, giving rise to cloudy conditions. This, together with instrumental problems, significantly reduced the number of days when formaldehyde could be evaluated with acceptable accuracy. In addition, real-time evaluation was only available for the SOF measurements, while the Mobile DOAS measurements were performed in offline mode. Hence, the SOF results guided the measurements, and formaldehyde results could only be analyzed after the campaign. As a result, a large portion of the measurements were performed in areas where no significant formaldehyde emissions were detected.

**Table 4.** A Day-by-Day Summary of All Formaldehyde Measurements at the Five Sources Repeatedly Detected During the SHARP Campaign[a]

| Source | Day | *N* | Time Period | Mean (kg/h) | SD (kg/h) | WS (m/s) | Range WD (deg) | |
|---|---|---|---|---|---|---|---|---|
| A | | | | | | | | |
| | 2009-04-22 | 7 | 11:39–18:26 | 15.3 | 3.0 | 9.9 | 200 | 208 |
| | 2009-04-23 | 1 | 15:51–15:53 | 15.9 | - | 11.5 | 161 | 161 |
| | 2009-05-04 | 1 | 18:03–18:05 | 10.8 | - | 2.9 | 101 | 101 |
| | 2009-05-13 | 3 | 17:00–18:49 | 15.6 | 6.0 | 9.8 | 173 | 173 |
| **Total** | | **12** | | **15.0** | **3.6** | **9.4** | **101** | **208** |
| B | | | | | | | | |
| | 2009-04-22 | 5 | 11:34–18:23 | 5.3 | 3.3 | 9.7 | 200 | 208 |
| | 2009-04-23 | 1 | 15:48–15:50 | 11.9 | - | 11.5 | 161 | 161 |
| | 2009-05-04 | 2 | 16:56–18:08 | 5.8 | 2.6 | 2.9 | 101 | 101 |
| | 2009-05-13 | 3 | 17:03–18:43 | 6.0 | 2.6 | 9.8 | 173 | 173 |
| **Total** | | **11** | | **6.2** | **3.2** | **8.7** | **101** | **208** |
| C | | | | | | | | |
| | 2009-05-15 | 1 | 18:07–18:11 | 11.5 | - | 7.5 | 151 | 151 |
| | 2009-05-16 | 1 | 16:38–16:44 | 22.6 | - | 7.4 | 163 | 163 |
| | 2009-05-18 | 7 | 10:34–16:21 | 7.6 | 1.9 | 4.7 | 28 | 28 |
| | 2009-05-19 | 4 | 10:10–16:11 | 11.3 | 4.3 | 5.2 | 80 | 80 |
| | 2009-05-20 | 3 | 17:11–17:36 | 6.9 | 2.4 | 3.2 | 19 | 19 |
| | 2009-05-29 | 3 | 14:00–16:52 | 14.8 | 10.9 | 2.7 | 7 | 347 |
| | 2009-05-30 | 2 | 11:42–12:12 | 15.7 | 5.8 | 2.6 | 117 | 321 |
| | 2009-06-05 | 1 | 11:58–12:01 | 9.7 | - | 2.7 | 27 | 27 |
| **Total** | | **22** | | **10.9** | **5.8** | **4.3** | **7** | **347** |
| D | | | | | | | | |
| | 2009-05-15 | 1 | 18:15–18:16 | 10.6 | - | 7.5 | 151 | 151 |
| | 2009-05-16 | 1 | 16:43–16:46 | 11.2 | - | 7.3 | 163 | 163 |
| | 2009-05-18 | 8 | 10:31–16:17 | 7.5 | 3.2 | 4.7 | 28 | 28 |
| | 2009-05-19 | 3 | 10:04–16:16 | 7.1 | 0.9 | 5.2 | 80 | 80 |
| | 2009-05-20 | 2 | 17:18–17:33 | 5.7 | 0.2 | 3.2 | 19 | 19 |
| | 2009-05-30 | 1 | 11:44–11:49 | 13.4 | - | 2.9 | 117 | 117 |
| **Total** | | **16** | | **8.0** | **3.0** | **5.0** | **19** | **163** |
| E | | | | | | | | |
| | 2009-05-18 | 1 | 18:32–18:34 | 33.4 | - | 4.7 | 28 | 28 |
| | 2009-05-20 | 1 | 18:41–18:43 | 53.4 | - | 3.2 | 19 | 19 |
| | 2009-06-05 | 1 | 08:16–08:18 | 49.8 | - | 5.6 | 48 | 48 |
| | 2009-04-20 | 1 | 17:31–17:33 | 19.7 | - | 6.4 | 4 | 4 |
| | 2009-05-28 | 2 | 17:26–18:27 | 40.5 | 32.5 | 3.3 | 14 | 33 |
| **Total** | | **6** | | **39.6** | **18.9** | **4.4** | **4** | **48** |

[a]*N* is the number of traverses, the time period for the measurements is given in the format HH:MM CDT, Mean and SD are the average and standard deviation of the calculated fluxes, and WS and WD are wind speed and wind direction. Day is given in the format year-month-day.

For these reasons, the measurements presented here come from only 15 of the 38 measurement days. Figure 3 shows the locations of five distinct formaldehyde sources, marked with the letters A–E, which were detected repeatedly in the Mobile DOAS measurements. The sources were identified purely based on the measurements and were not known beforehand. The approximate locations of the sources were inferred based on measurements in different wind directions but could not be pinpointed to specific point sources in the emitting facilities. All together 68 flux measurements were made on plumes from these sources. A clear majority of these measurements, 41, were made during 4 days: 22 April and 18–20 May. These were days with clear skies, a problem-free DOAS instrument, and a measurement focus on areas with distinct formaldehyde sources. The results of these measurements are summarized in Table 4. The average formaldehyde flux measured from the two sources in Texas City was approximately 15 and 6 kg/h, respectively, while the two sources in Mont Belvieu had fluxes of approximately 11 and 8 kg/h, and the single source in HSC had an average measured flux of approximately 40 kg/h. These results were used in *Parrish et al.* [2012] as an estimate of the total primary formaldehyde emissions in these areas.

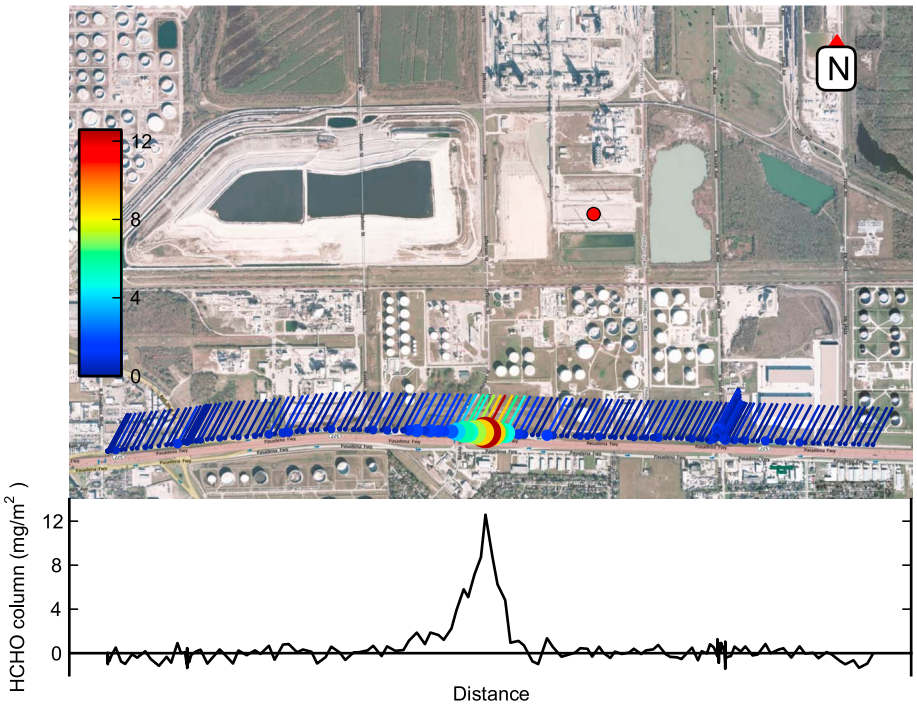


**Figure 7.** Measurements of a formaldehyde plume from source E in Houston Ship Channel. Each circle corresponds to one Mobile DOAS spectrum, and the size and color of the circle indicate the magnitude of the HCHO column evaluated from the spectrum. A line from each circle indicates the direction the wind is blowing from. The plume profile of formaldehyde is also plotted below.

As described in section 2.2, emission plumes are identified as peaks in the column concentration time series for one or several species. An example of an isolated peak is shown in Figure 7. This is a formaldehyde measurement of a plume from source E around 18:33 CDT on 18 May 2009. The formaldehyde flux in this plume was calculated to be approximately 33 kg/h. The plumes studied here typically had ground

**Table 5.** A Day-by-Day Summary of Formaldehyde Measurements During the Follow-Up Measurements Made in April 2011[a]

| Source | Day | *N* | Time Period | Mean (kg/h) | SD (kg/h) | WS (m/s) | Range WD (deg) | |
|---|---|---|---|---|---|---|---|---|
| A | | | | | | | | |
| | 2011-04-17 | 16 | 14:38–18:20 | 25.4 | 13.7 | 10.7 | 146 | 146 |
| B | | | | | | | | |
| | 2011-04-17 | 9 | 15:32–18:05 | 14.8 | 10.0 | 10.7 | 146 | 146 |
| X | | | | | | | | |
| | 2011-04-17 | 14 | 14:40–18:19 | 9.5 | 6.7 | 10.7 | 146 | 146 |
| C | | | | | | | | |
| | 2011-04-16 | 4 | 17:54–18:21 | 18.8 | 5.1 | 3.5 | 0 | 355 |
| | 2011-04-27 | 2 | 17:29–17:54 | 20.8 | 8.3 | 10.1 | 314 | 331 |
| **Total** | | **6** | | **19.5** | **5.5** | **5.7** | **314** | **335** |
| E | | | | | | | | |
| | 2011-04-15 | 1 | 13:04–13:06 | 24.0 | - | 10.3 | 325 | 325 |
| | 2011-04-16 | 7 | 09:46–16:30 | 45.7 | 38.8 | 6.9 | 4 | 359 |
| | 2011-04-28 | 4 | 10:59–16:36 | 14.6 | 7.3 | 4.6 | 17 | 35 |
| **Total** | | **12** | | **33.6** | **32.7** | **6.4** | **4** | **359** |
| Y | | | | | | | | |
| | 2011-04-15 | 1 | 18:19–18:22 | 76.8 | - | 9.8 | 322 | 322 |
| | 2011-04-16 | 2 | 13:37–15:08 | 18.8 | 0.7 | 4.5 | 38 | 323 |
| | 2011-04-28 | 3 | 11:34–14:32 | 22.8 | 14.5 | 5.0 | 15 | 34 |
| **Total** | | **6** | | **30.5** | **24.6** | **5.6** | **15** | **323** |

[a]Two new sources detected are referred to as X (Texas City) and Y (HSC). *N* is the number of traverses, the time period for the measurements is given in the format HH:MM CDT, Mean and SD are the average and standard deviation of the calculated fluxes, and WS and WD are wind speed and wind direction. Day is given in the format year-month-day.

**Table 6.** Comparison of the Average HCHO Fluxes Measured From All Sources in 2009 and 2011[a]

| | Average Flux (kg/h) | | | | | | | |
|---|---|---|---|---|---|---|---|---|
| Year | A | B | C | D | E | X | Y | Total |
| 2009 | 15.0 | 6.2 | 10.9 | 8.0 | 39.6 | - | - | 79.7 |
| 2011 | 25.4 | 14.8 | 19.5 | - | 33.6 | 9.5 | 30.5 | 133.3 |

[a]A–E are the sources found in 2009, while X and Y are the two new sources found in 2011.

widths of a few hundred meters up to 1 km. Variations in column concentrations on larger time scales also exist in the data set but are more difficult to interpret. Possible explanations are variations in background HCHO, large-scale plumes and changes in path of the scattered light. Any significant HCHO point source should, however, be possible to detect as a plume of this approximate width if measurements are made within 1–2 km downwind.

In April 2011, the same Mobile DOAS setup was partly used to follow-up the 2009 study as a part of the AQRP study [*Johansson et al.*, 2011]. A summary of all the HCHO measurements in 2011 is shown in Table 5. Overall, the 2011 measurements showed rather similar results to 2009. Although there were fewer measurement days in 2011, all sources found in 2009 were also detected in 2011 except source D. This was at least partly due to unfavorable wind directions for this source, making it more difficult to detect. In addition to the sources detected in 2009, two new sources were detected: source X, located in Texas City and source Y, near the southwest end of the Fred Hartman Bridge in HSC. The locations of these sources have also been marked in Figure 3. A comparison between the average fluxes measured from the different sources in 2009 and 2011 is shown in Table 6. The measured fluxes were mostly higher in 2011, especially in Texas City, but due to the limited number of measurements and the variation between them, it is not clear that this is due to a long-term change. The sum of the average fluxes measured in 2011 was 133 kg/h, as opposed to 80 kg/h in 2009. However, most of the difference between these 2 years is explained by the new source Y which showed an average emission of 31 kg/h in 2011 but was not detected at all in 2009. Apart from this new source, the general picture of the industrial HCHO emissions did not seem to have changed from 2009 to 2011.

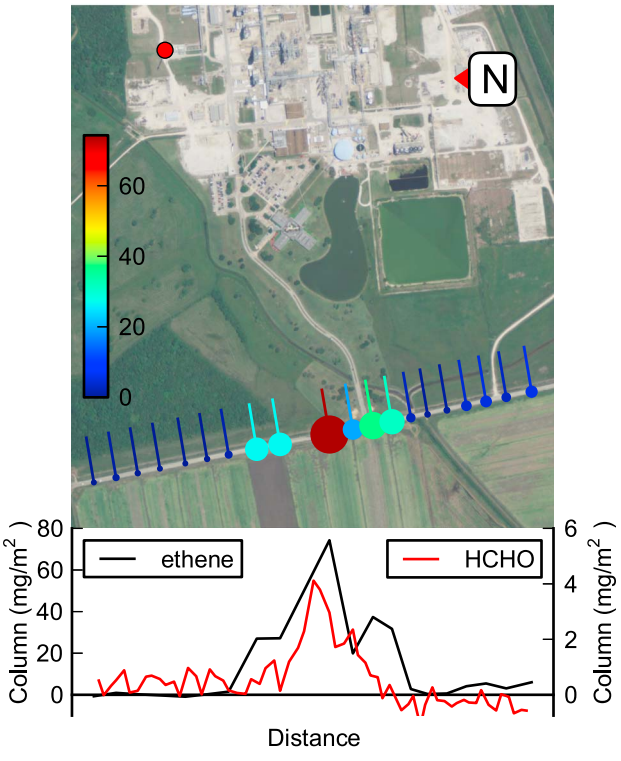


**Figure 8.** Measurements of a plume from source D in northern Mont Belvieu. Each circle corresponds to one SOF spectrum, and the size and color of the circle indicate the magnitude of the ethene column evaluated from the spectrum. A line from each circle indicates the direction the wind is blowing from, and a red circle indicates the location of a flare suspected to be the source. The plume profiles of ethene and formaldehyde are also plotted below.

### 3.2. Primary Versus Secondary Formaldehyde (Plume Chemistry Modeling)

The formaldehyde plumes presented in section 3.1 were generally detected close to their presumed sources (typically 500–2000 m downwind). While formaldehyde is known to be formed secondarily from oxidation of alkenes, and previous studies have shown that there are large emissions of alkenes in these areas [*Mellqvist et al.*, 2010], it is questionable whether the amounts of formaldehyde measured could be formed secondarily in such a short time. Even with an abundance of alkenes or other VOCs, there is a question of whether there are enough OH radicals available to oxidize them at a sufficient rate. To answer this question the plume chemistry model described in section 2.6 was used to

**Table 7.** Summary of the Input Parameters and Simulation Results for the 13 Cases the Plume Chemistry Model was Applied to[a]

| | | | | Flux (kg/h) | | | | | | | |
|---|---|---|---|---|---|---|---|---|---|---|---|
| Case | Source | Date | Time (CDT) | Ethene | Propene | Alkanes | $NO_2$ | $SO_2$ | Total HCHO | Primary HCHO | Secondary HCHO |
| 1 | A | 2009-04-22 | 11:38 | 84.7 | 90.0 | 839.8 | 19.7 | 162.7 | 19.00 | 17.95 | 1.06 |
| 2 | C | 2009-05-18 | 10:34 | - | 17.8 | 539.5 | 39.2 | - | 6.20 | 6.22 | −0.02 |
| 3 | C | 2009-05-18 | 11:39 | 35.4 | 40.8 | 2290.7 | 61.3 | - | 8.70 | 8.37 | 0.33 |
| 4 | C | 2009-05-18 | 14:42 | 59.8 | - | 213.3 | 28.4 | - | 4.00 | 3.88 | 0.12 |
| 5 | C | 2009-05-18 | 14:50 | 35.6 | - | 85.9 | 37.4 | - | 9.60 | 9.57 | 0.03 |
| 6 | D | 2009-05-18 | 10:30 | 36.5 | - | 66.3 | 4.3 | - | 5.50 | 5.21 | 0.29 |
| 7 | D | 2009-05-18 | 15:02 | 61.7 | - | 112.7 | - | - | 5.10 | 5.00 | 0.10 |
| 8 | D | 2009-05-19 | 10:04 | 489.0 | 47.2 | 712.0 | 11.2 | - | 7.45 | 4.22 | 3.23 |
| 9 | D | 2009-05-19 | 15:11 | 232.0 | - | 388.2 | - | - | 7.90 | 7.46 | 0.44 |
| 10 | D | 2009-05-19 | 16:13 | 845.0 | 51.4 | 1782.3 | - | - | 6.10 | 5.05 | 1.05 |
| 11 | D | 2009-05-20 | 17:15 | 275.0 | - | 337.0 | 8.9 | - | 14.20 | 12.97 | 1.23 |
| 12 | E | 2009-05-25 | 11:35 | 179.0 | - | 422.0 | 53.9 | - | 50.00 | 44.25 | 5.75 |
| 13 | E | 2009-05-28 | 18:22 | 42.2 | - | 143.0 | 61.6 | - | 17.20 | 17.40 | −0.20 |

[a]The measured fluxes of ethene, propene, alkanes, $NO_2$, $SO_2$, and HCHO are shown together with primary and secondary HCHO emissions as given by the simulations. Time and date of the measurements as well as the source of the emissions are also given.

model the cases from 2009 where a plume of ethene and/or propene had been detected with SOF at the same time and location as one of the formaldehyde plumes in section 3.1.

As an example, Figure 8 shows a measurement transect on 19 May 2009 west of source D in Mont Belvieu. Here an ethene flux of 232 kg/h was measured at the same location as a formaldehyde flux of 7.9 kg/h. This is one of the largest ethene sources detected in the study, and a flare in a nearby petrochemical industry was suspected to be the emitter. Measurements were performed on the same flare a few days earlier by the Aerodyne mobile lab [*Wood et al.*, 2012], showing an ethene to formaldehyde mass ratio of 105:1. This can be compared to the equivalent mass ratios for the same source in this study, which varied between 6:1 and 140:1 in six independent flux measurement transects (see Table 7). These nearly coincident measurements hence support the conclusion that formaldehyde is released from a flare in this case.

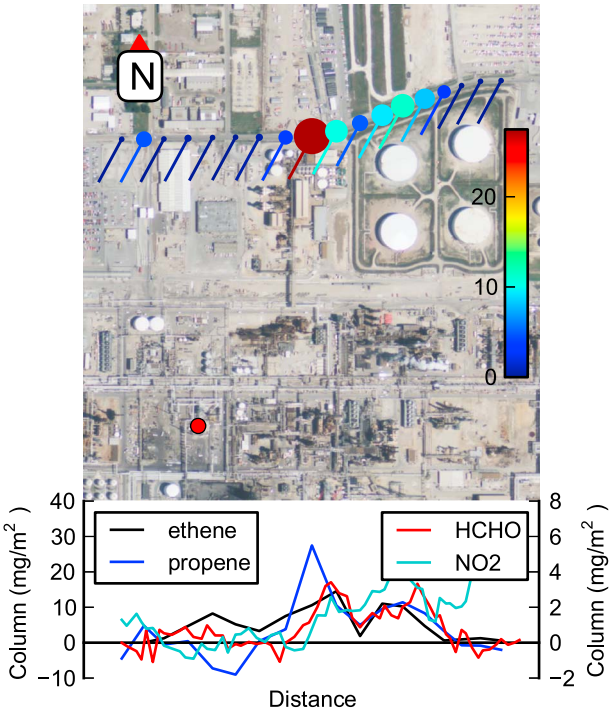


**Figure 9.** Measurements of a plume from source A in Texas City. Each circle corresponds to one SOF spectrum, and the size and color of the circle indicate the magnitude of the propene column evaluated from the spectrum. A line from each circle indicates the direction the wind is blowing from, and a red circle indicates the location of a flare suspected to be the source. The plume profiles of ethene, propene, formaldehyde, and $NO_2$ are also plotted below.

Figure 9 shows another example, a traverse on the north side of the Texas City industrial area on 22 April 2009. Fluxes of 85 kg/h ethene, 90 kg/h propene, 19 kg/h formaldehyde, 20 kg/h $NO_2$, and 163 kg/h $SO_2$ were measured at the same location. Since this was the largest $SO_2$ emission detected in the area, a nearby flare reporting the largest $SO_2$ emissions was suspected to be the source. This particular source was also investigated by *Olaguer et al.* [2013] using inverse dispersion modeling based on measurements by the Aerodyne mobile lab [*Kolb et al.*, 2004] on 13 May 2009. The model attributed HCHO emissions of roughly 22 kg/h in total from a number of sources located in the same approximate area, in good agreement with

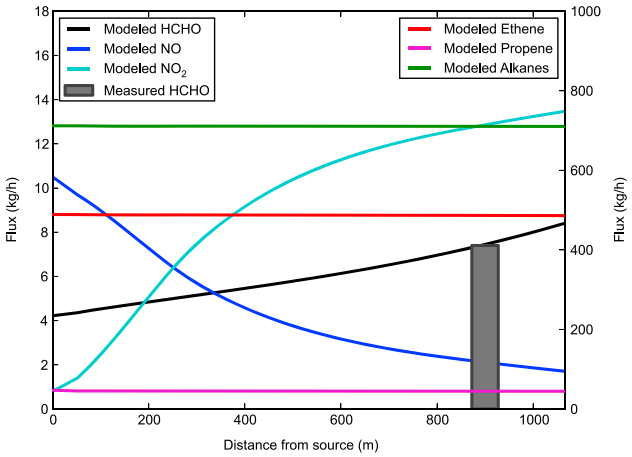


**Figure 10.** Results from the plume chemistry simulation case showing the largest fraction of secondary HCHO. Modeled fluxes of HCHO (primary + secondary), NO, $NO_2$ (on the left *y* axis), ethene, propene, and alkanes (on the right *y* axis) as a function of downwind distance from the source. The primary HCHO emission rate (i.e., the initial HCHO flux) was iteratively determined in order to get the right total HCHO flux at the measurement distance.

the 15.6 ± 6.0 kg/h HCHO measured with Mobile DOAS on the same day (see source A in Table 4). *Stutz et al.* [2011] also carried out MAX-DOAS measurements downwind of this source and found a strong correlation between $SO_2$ and HCHO, especially in the period 12–14 May, indicating that the HCHO emissions are colocated with the largest $SO_2$ sources in the area. This is also consistent with the measurements for source A in this study.

Altogether, 13 collocated measurements of formaldehyde and ethene and/or propene were identified. This leaves most of the formaldehyde plumes not having been detected together with alkenes. To some extent this was due to the SOF instrument not always measuring at the time of formaldehyde detection or not performing well enough to give accurate measurements. However, some of the formaldehyde plumes detected were definitely not accompanied with any significant amounts of ethene or propene. No apparent correlation was found between the size of the HCHO mass flux and the presence of ethene or propene. Still, the 13 cases of collocated formaldehyde and alkene plumes were modeled to determine if oxidation of the alkenes could explain the formaldehyde emission seen. Since SOF and Mobile DOAS do not measure along the same light path, it is generally not possible to determine conclusively whether or not the formaldehyde and the alkenes are in the same plume. The modeling was, however, based on the assumption that they were.

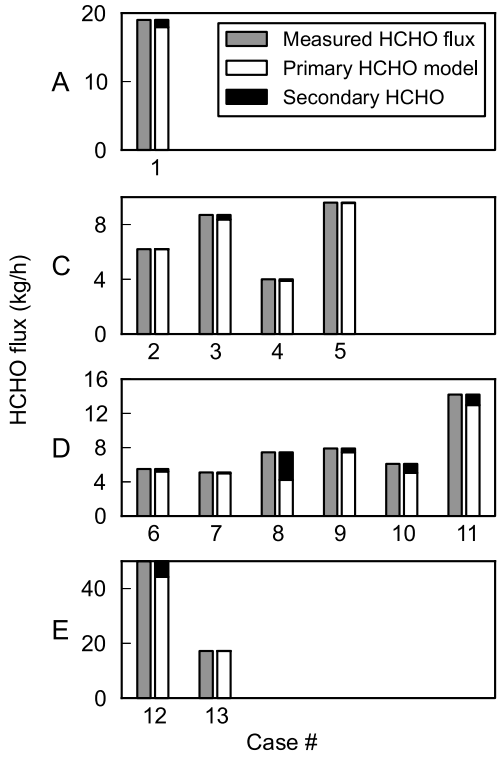


**Figure 11.** Measured HCHO fluxes for the 13 plume chemistry simulation cases and the fraction of it explained by primary and secondary emissions, respectively, according to the results. The cases are sorted by the emission source from which the plume was detected.

Figure 10 shows the fluxes of HCHO, NO, $NO_2$, ethene, propene, and alkanes as a function of downwind distance from the source in simulation case 8. Approximately 43% of the measured HCHO flux was explained by secondary emissions according to the model. The VOC levels (ethene, propene, and alkanes) clearly remain almost constant on this time scale, while most of the NO is converted to $NO_2$. Even though the fraction of VOCs degraded is very small, the HCHO produced from this is still a significant part of the HCHO measured. This is due to the VOC and HCHO fluxes differing by approximately 2 orders of magnitude.

Table 7 shows the measured emission fluxes used for each of the simulations together with the results in terms of primary and secondary HCHO. In a few cases the secondary HCHO is negative. This means that more formaldehyde was degraded than produced in the simulation.

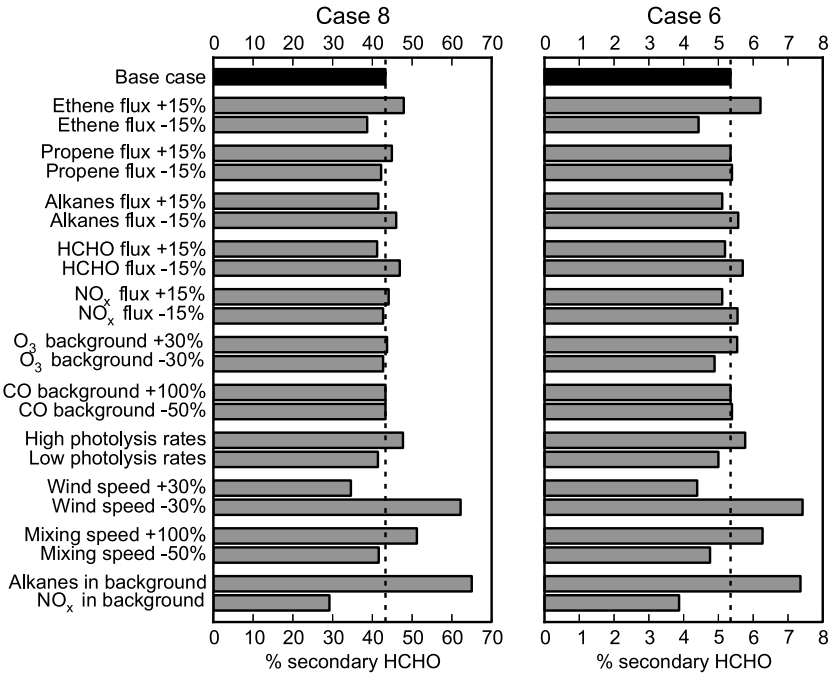


**Figure 12.** Percentage of the measured HCHO flux attributed to secondary emissions in each of the scenarios in the sensitivity analysis of the modeling results for case 8, which had the highest primary HCHO percentage, 43%, and case 6, which was more typical with 5% primary HCHO.

Figure 11 shows how much of the measured formaldehyde flux is explained as primary and secondary emissions, respectively, in each of the 13 cases, sorted by source. The secondary emissions account for less than 10% of the measured HCHO flux in most cases and only in case 8 discussed above does it account for more than 20%.

In order to test the robustness of the modeling results with respect to the input parameters, a series of simulations were run with perturbations of the input parameters on the approximate scale of the uncertainty of these parameters. This gave an approximation of the uncertainty in the results of the simulations as well as an indication of which parameters the model is most sensitive to. Each of the measured fluxes (ethene, propene, alkanes, HCHO, and $NO_2$) were perturbed with ±15%, representing the nonwind-dependent uncertainty of the flux measurement. The background concentration of $O_3$ was perturbed by ±30%, and the background concentration of CO was perturbed with +100% and −50%. Perturbations of the photolysis rates used the 90th and 50th percentile values for a given SZA instead of the 70th percentile, and the vertical mixing speed was perturbed with +100% and −50%. Wind speed perturbations of ±30% were applied, but this perturbation was also applied to all the measured fluxes since the wind speed was used to calculate these fluxes. Hence, the effect of increasing the wind speed in the model, for example, was the combined effect of increasing the fluxes in the model and decreasing transport time. Finally, the possibility that the alkanes and the $NO_x$ fluxes measured were not from the same source as the alkenes and HCHO was considered. This scenario was approximated by separately adding $NO_x$ and alkanes as background concentrations instead, using the concentrations of these at the measurement point in the original simulation.

These perturbations were applied to case 6, which was a fairly typical case with approximately 5% secondary HCHO in the original simulation, and to case 8, which showed the highest percentage of secondary HCHO of all cases, 42%. The result of all these perturbations as applied to simulation cases 6 and 8 is shown in Figure 12. Apparently, the largest effects come from the perturbations of the wind speed and from moving $NO_x$ and alkanes to the background. Lower wind speed gives longer transport time and lower total HCHO flux measured, both of which should increase the percentage of secondary emission. On the other hand, lower wind speed also gives lower VOC and $NO_x$ fluxes which should decrease the secondary emissions. The combined effect of a decrease of the wind speed by 30% was an increase in secondary emissions from approximately 43% to 62% in case 8 and from 5% to 7% in case 6. Turning the alkanes into a background

species lowers the concentrations of them, especially in the beginning of the simulation when the plume is more concentrated. This allows more of the OH radicals available in the plume to react with alkenes, which gives secondary HCHO. This is the reason for the increase from 43% to 65% secondary HCHO seen for this perturbation in case 8 and from 5% to 7% in case 6. Similarly, moving the $NO_x$ flux to the background decreases the secondary HCHO emissions because less NO is available to turn $HO_2$ into OH. Smaller effects are observed from the perturbations of the individual fluxes, the photolysis rates, and the vertical mixing speed, while the changes in background concentrations of $O_3$ and CO made almost no difference. Comparing the results of the perturbations in case 6 and case 8, it seems that the changes were roughly proportional to the original secondary HCHO fraction. Even though some of the perturbation caused significant changes in the secondary HCHO fraction, the maximum combined effect of all perturbations will not give much more than double the original HCHO fraction. For case 8 it could therefore be conceivable that all or most of the formaldehyde is secondary, but for all the other cases doubling the secondary HCHO fraction would at least still leave over 60% of the HCHO as primary emissions. The conclusion is that the modeling results are robust enough to show that the HCHO emissions measured with the Mobile DOAS system are at least for the most part primary.

## 4. Conclusions and Discussion

A new sensitive mobile DOAS system for fast real-time emission measurements of HCHO, $NO_2$, and $SO_2$ has been demonstrated with a detection limit of 3 ppb HCHO over a 100 m altitude layer. During good measurement conditions plumes with HCHO fluxes of approximately 5 kg/h and upward could be detected at distances of 500–2000 m, where they had typical widths of 100–500 m. The system has been operated together with a Solar Occultation Flux (SOF) system for VOC emission measurements with overall measurement uncertainties of 30% for both systems. Since the optical remote sensing techniques used here facilitates efficient top-down emission screening of large industrial areas, they enabled a comprehensive survey of industries in HSC, Texas City, and Mont Belvieu and identified the major local HCHO sources. The large coverage does not, however, necessarily mean that all primary industrial formaldehyde sources were detected in this study. Successful detection of a source is dependent on weather conditions, proximity to the source when passing the plume, and the magnitude of the formaldehyde flux. We estimate, based on the conditions under which plumes were detected, that for most of the major refining and petrochemical facilities in the areas, conditions were good enough to detect plumes of 5 kg/h and upward, at least a couple of times during the two studies. This leaves the possibility of smaller sources having remained undetected during the study. In the three surveyed areas, HCHO emissions were repeatedly detected from seven distinct sources over the 2 years studied, with a median emission rate of 15 kg/h spanning between 5 to 75 kg/h and an accumulated emission rate of approximately 120 kg/h. In a parallel study during the 2009 campaign, *Pikelnaya et al.* [2013] detected primary formaldehyde in plumes from three different flares in the same areas using Imaging DOAS. The HCHO fluxes from these flares were quantified to be approximately 0.8 kg/h, 0.2 kg/h, and 8 kg/h, respectively. This indicates that some flares have smaller HCHO emissions than the ones found in this study. The smaller HCHO fluxes (0.8 kg/h and 0.2 kg/h) would not be possible to detect with the Mobile DOAS measurements described in this study, and hence, the total HCHO emissions might be somewhat higher than 120 kg/h. It is unlikely, however, that these smaller formaldehyde sources together outweigh the emissions of the larger sources detected with Mobile DOAS, given the limited number of burning flares in these areas. In comparison, total primary HCHO emissions from on-road vehicles in the HGB area was estimated by *Parrish et al.* [2012] to be approximately 75 kg/h.

In many cases significant alkene emissions were detected simultaneously with the HCHO plumes and these VOC emissions were typically an order of magnitude larger than the HCHO emissions. Most of these alkene emissions will, however, form secondary HCHO further downwind. A Lagrangian plume model was applied to investigate to what extent the measured HCHO emissions were primary or secondary emissions. The model results showed that primary emissions typically account for around 90% of the measured HCHO, with only a few cases showing significant photochemical production of HCHO. A sensitivity analysis of the model indicates that assumptions of the spatial origin of the alkane emission sources and the magnitude of the wind speed are the largest sources of uncertainty in the results. For a few cases with a significant secondary HCHO fraction this might increase the fraction of secondary HCHO even more, but in most modeled cases the difference would be negligible. Complementary studies by *Wood et al.* [2012], *Olaguer et al.* [2013], and *Stutz et al.* [2011] were carried out at some of the sources investigated during the same time period and supports the interpretation that the primary HCHO is emitted from flare stacks.

Although the plume chemistry model showed that 90% of the formaldehyde measured was typically primary emissions at downwind distances of 500–2000 m, this does not mean that primary industrial emissions dominate over secondary on a larger scale in the HGB area. The results of this study rather points in the opposite direction. Total routine primary emissions of HCHO is not likely to be significantly larger than the approximately 120 kg/h identified. By contrast, according to *Mellqvist et al*. [2010] and *Johansson et al*. [2014] total industrial emissions of ethene and propene from the same areas are more than 1000 kg/h each. Based on the assumption of complete degradation of those alkene emissions *Parrish et al*. [2012] estimated the total secondary industrial formaldehyde emissions from these areas to be approximately 2260 kg/h. Hence, secondary formaldehyde should be assumed to outweigh primary by at least an order of magnitude further downwind of the emission sources. This was confirmed qualitatively by running the plume chemistry simulations in this study further downwind past the measurement points, which typically resulted in secondary formaldehyde dominating over primary at some point. However, due to the time needed for secondary formaldehyde to be formed, primary formaldehyde emissions might be expected to have a larger impact on areas close to the emission sources, while the impact of the secondary formaldehyde is distributed over a larger region.

**Acknowledgments**

The 2009 measurements were funded by Texas Environmental Research Consortium (TERC) under project H102. The 2011 measurements were funded by state of Texas through the Air Quality Research Program administered by the University of Austin under project 10-006. The additional data analysis and funding for writing this paper was obtained by additional financial support by TCEQ under a separate contract. The authors would like to thank Mattias Johansson for technical assistance with the HCHO evaluation and TCEQ for supplying wind data.

## References

Bogumil, K., et al. (2003), Measurements of molecular absorption spectra with the SCIAMACHY pre-flight model: Instrument characterization and reference data for atmospheric remote-sensing in the 230–2380 nm region, *J. Photochem. Photobiol., A*, *157*(2–3), 167–184, doi:10.1016/S1010-6030(03)00062-5.

Burrows, J. P., A. Dehn, B. Deters, S. Himmelmann, A. Richter, S. Voigt, and J. Orphal (1998), Atmospheric remote-sensing reference data from GOME: Part 1. Temperature-dependent absorption cross-sections of $NO_2$ in the 231-794 nm range, *J. Quant. Spectros. Radiat. Transfer*, *60*(6), 1025–1031, doi:10.1016/S0022-4073(97)00197-0.

Burrows, J. P., A. Richter, A. Dehn, B. Deters, S. Himmelmann, S. Voigt, and J. Orphal (1999), Atmospheric remote-sensing reference data from GOME—2. Temperature-dependent absorption cross sections of $O_3$ in the 231-794 nm range, *J. Quant. Spectros. Radiat. Transfer*, *61*(4), 509–517.

Buzcu Guven, B., and E. P. Olaguer (2011), Ambient formaldehyde source attribution in Houston during TexAQS II and TRAMP, *Atmos. Environ.*, *45*(25), 4272–4280, doi:10.1016/j.atmosenv.2011.04.079.

Cantrell, C. A., J. A. Davidson, A. H. McDaniel, R. E. Shetter, and J. G. Calvert (1990), Temperature-dependent formaldehyde cross sections in the near-ultraviolet spectral region, *J. Phys. Chem.*, *94*(10), 3902–3908.

De Gouw, J. A., et al. (2009), Airborne measurements of ethene from industrial sources using laser photo-acoustic spectroscopy, *Environ. Sci. Technol.*, *43*(7), 2437–2442, doi:10.1021/es802701a.

Derwent, R. G., and M. E. Jenkin (1990), Hydrocarbon involvement in photochemical ozone formation in Europe, *Rep. AERE-report-R 13736*, London.

Fayt, C. (2011), QDOAS (Version 1.00) [software], Belgian Institute for Space Aeronomy Brussles, Belgium.

Friedfeld, S., M. Fraser, K. Ensor, S. Tribble, D. Rehle, D. Leleux, and F. Tittel (2002), Statistical analysis of primary and secondary atmospheric formaldehyde, *Atmos. Environ.*, *36*(30), 4767–4775, doi:10.1016/S1352-2310(02)00558-7.

Galle, B., C. Oppenheimer, A. Geyer, A. J. S. McGonigle, M. Edmonds, and L. Horrocks (2002), A miniaturised ultraviolet spectrometer for remote sensing of $SO_2$ fluxes: A new tool for volcano surveillance, *J. Volcanol. Geotherm. Res.*, *119*(1-4), 241–254, doi:10.1016/S0377-0273(02)00356-6.

Gery, M. W., G. Z. Whitten, J. P. Killus, and M. C. Dodge (1989), A photochemical kinetics mechanism for urban and regional scale computer modeling, *J. Geophys. Res.*, *94*(D10), 12,925–12,956.

Gilman, J. B., et al. (2009), Measurements of volatile organic compounds during the 2006 TexAQS/GoMACCS campaign: Industrial influences, regional characteristics, and diurnal dependencies of the OH reactivity, *J. Geophys. Res.*, *114*, D00F06, doi:10.1029/2008JD011525.

Haeger-Eugensson, M., J. Moldanova, M. Ferm, M. Jerksjö, and E. Fridell (2010), On the increasing levels of $NO_2$ in some cities. The role of primary emissions and shipping, *Rep.*, IVL Swedish Environmental Research Institute.

Hanna, S. R., G. A. Briggs, and R. P. J. Hosker (1982), *Handbook on Atmospheric Diffusion*, Rep. DOE/TIC-11223; Other: ON: DE82002045, 107 pp., National Oceanic and Atmospheric Administration, Oak Ridge, Tenn.

Hermans, C., A. C. Vandaele, M. Carleer, S. Fally, R. Colin, A. Jenouvrier, B. Coquart, and M. F. Mérienne (1999), Absorption cross-sections of atmospheric constituents: $NO_2$, $O_2$, and $H_2O$, *Environ. Sci. Pollut. Res.*, *6*(3), 151–158.

Ibrahim, O., R. Shaiganfar, R. Sinreich, T. Stein, U. Platt, and T. Wagner (2010), Car MAX-DOAS measurements around entire cities: Quantification of $NO_x$ emissions from the cities of Mannheim and Ludwigshafen (Germany), *Atmos. Meas. Tech.*, *3*(3), 709–721, doi:10.5194/amt-3-709-2010.

Jobson, B. T., C. M. Berkowitz, W. C. Kuster, P. D. Goldan, E. J. Williams, F. C. Fesenfeld, E. C. Apel, T. Karl, W. A. Lonneman, and D. Riemer (2004), Hydrocarbon source signatures in Houston, Texas: Influence of the petrochemical industry, *J. Geophys. Res.*, *109*, D24305, doi:10.1029/2004JD004887.

Johansson, J. K. E., J. Mellqvist, J. Samuelsson, B. Offerle, B. Rappenglück, D. Anderson, B. Lefer, S. Alvarez, and J. Flynn (2011), Quantification of industrial emissions of VOCs, $NO_2$ and $SO_2$ by SOF and Mobile DOAS, *Rep. 10-006*, Air Quality Research Program, University of Texas at Austin.

Johansson, J. K. E., J. Mellqvist, J. Samuelsson, B. Offerle, B. Lefer, B. Rappenglück, J. Flynn, and G. Yarwood (2014), Emission measurements of alkenes, alkanes, $SO_2$, and $NO_2$ from stationary sources in Southeast Texas over a 5 year period using SOF and mobile DOAS, *J. Geophys. Res. Atmos.*, *119*, 1973–1991, doi:10.1002/2013JD020485.

Johansson, M., B. Galle, T. Yu, L. Tang, D. Chen, H. Li, J. X. Li, and Y. Zhang (2008), Quantification of total emission of air pollutants from Beijing using mobile mini-DOAS, *Atmos. Environ.*, *42*(29), 6926–6933, doi:10.1016/j.atmosenv.2008.05.025.

Johansson, M., C. Rivera, B. DeFoy, W. Lei, J. Song, Y. Zhang, B. Galle, and L. Molina (2009), Mobile mini-DOAS measurement of the outflow of $NO_2$ and HCHO from Mexico City, *Atmos. Chem. Phys.*, *9*(15), 5647–5653, doi:10.1029/2005GL022616.

Karl, T., T. Jobson, W. C. Kuster, E. Williams, J. Stutz, R. Shetter, S. R. Hall, P. Goldan, F. Fehsenfeld, and W. Lindinger (2003), Use of proton-transfer-reaction mass spectrometry to characterize volatile organic compound sources at the La Porte super site during the Texas Air Quality Study 2000, *J. Geophys. Res.*, *108*(16), 4368, doi:10.1029/2002JD002967.

Kleinman, L. I., P. H. Daum, D. Imre, Y. N. Lee, L. J. Nunnermacker, S. R. Springston, J. Weinstein-Lloyd, and J. Rudolph (2002), Ozone production rate and hydrocarbon reactivity in 5 urban areas: A cause of high ozone concentration in Houston, *Geophys. Res. Lett.*, *29*(10), 1467, doi:10.1029/2001GL014569.

Klug, W. (1969), Method for determining atmospheric dispersion conditions from synoptic observations, *Staub-Reinhalt. Luft*, *29*(4), 143–147.

Kolb, C. E., S. C. Herndon, J. B. McManus, J. H. Shorter, M. S. Zahniser, D. D. Nelson, J. T. Jayne, M. R. Canagaratna, and D. R. Worsnop (2004), Mobile laboratory with rapid response instruments for real-time measurements of urban and regional trace gas and particulate distributions and emission source characteristics, *Environ. Sci. Technol.*, *38*(21), 5694–5703, doi:10.1021/es030718p.

Kraus, S. (2004), DOASIS: DOAS Intelligent System (Version 3.2) [software], Univ. of Heidelberg, Heidelberg, Germany.

Kurucz, R. L. (1994), The solar spectrum: Atlases and line identifications, paper presented at Astronomical Society of the Pacific Conference Series, Astronomical Society of the Pacific, Brussels, 29 August - 2 September.

Lefer, B. (2009), Study of Houston Atmospheric Radical Precursors (SHARP), *Rep*. *H100*, Texas Environmental Research Consortium, Houston Advanced Research Center.

Meller, R., and G. K. Moortgat (2000), Temperature dependence of the absorption cross sections of formaldehyde between 223 and 323 K in the wavelength range 225-375 nm, *J. Geophys. Res.*, *105*(D6), 7089–7101.

Mellqvist, J., J. Samuelsson, J. K. E. Johansson, C. Rivera, B. Lefer, S. Alvarez, and J. Jolly (2010), Measurements of industrial emissions of alkenes in Texas using the solar occultation flux method, *J. Geophys. Res.*, *115*, D00F17, doi:10.1029/2008JD011682.

Moldanova, J. (2010), Report on ship plume simulations and analysis, *Rep*. *B1920*, IVL Swedish Environmental Research Institute, Gothenburg, Sweden.

Olaguer, E. P., S. C. Herndon, B. Buzcu-Guven, C. E. Kolb, M. J. Brown, and A. E. Cuclis (2013), Attribution of primary formaldehyde and sulfur dioxide at Texas City during SHARP/formaldehyde and olefins from large industrial releases (FLAIR) using an adjoint chemistry transport model, *J. Geophys. Res. Atmos.*, *118*, 11,317–11,326, doi:10.1002/jgrd.50794.

Parrish, D. D., et al. (2009), Overview of the second Texas Air Quality Study (TexAQS II) and the Gulf of Mexico atmospheric composition and climate study (GoMACCS), *J. Geophys. Res.*, *114*, D00F13, doi:10.1029/2009JD011842.

Parrish, D. D., et al. (2012), Primary and secondary sources of formaldehyde in urban atmospheres: Houston Texas region, *Atmos. Chem. Phys.*, *12*(7), 3273–3288, doi:10.5194/acp-12-3273-2012.

Pikelnaya, O., J. H. Flynn, C. Tsai, and J. Stutz (2013), Imaging DOAS detection of primary formaldehyde and sulfur dioxide emissions from petrochemical flares, *J. Geophys. Res. Atmos.*, *118*, 8716–8728, doi:10.1002/jgrd.50643.

Pinardi, G., et al. (2013), MAX-DOAS formaldehyde slant column measurements during CINDI: Intercomparison and analysis improvement, *Atmos. Meas. Tech.*, *6*(1), 167–185, doi:10.5194/amt-6-167-2013.

Platt, U., and J. Stutz (2008), *Differential Absorption Spectroscopy*, 597 pp., Springer, Berlin Heidelberg, doi:10.1007/978-3-540-75776-4.

Pszenny, A. A. P., J. Moldanová, W. C. Keene, R. Sander, J. R. Maben, M. Martinez, P. J. Crutzen, D. Perner, and R. G. Prinn (2004), Halogen cycling and aerosol pH in the Hawaiian marine boundary layer, *Atmos. Chem. Phys.*, *4*(1), 147–168, doi:10.1029/2001JD000943.

Rappenglück, B., P. K. Dasgupta, M. Leuchner, Q. Li, and W. Luke (2010), Formaldehyde and its relation to CO, PAN, and $SO_2$ in the Houston-Galveston airshed, *Atmos. Chem. Phys.*, *10*(5), 2413–2424, doi:10.1029/2008JD009865.

Rivera, C., G. Sosa, H. Wöhrnschimmel, B. De Foy, M. Johansson, and B. Galle (2009), Tula industrial complex (Mexico) emissions of $SO_2$ and $NO_2$ during the MCMA 2006 field campaign using a mobile mini-DOAS system, *Atmos. Chem. Phys.*, *9*(17), 6351–6361, doi:10.1029/2002GL015827.

Rivera, C., J. Mellqvist, J. Samuelsson, B. Lefer, S. Alvarez, and M. R. Patel (2010), Quantification of $NO_2$ and $SO_2$ emissions from the Houston Ship Channel and Texas City industrial areas during the 2006 Texas Air Quality Study, *J. Geophys. Res.*, *115*, D08301, doi:10.1029/2009JD012675.

Ryerson, T. B., et al. (2003), Effect of petrochemical industrial emissions of reactive alkenes and NO x on tropospheric ozone formation in Houston, Texas, *J. Geophys. Res.*, *108*(8), 4249, doi:10.1029/2002JD003070.

Shaiganfar, R., S. Beirle, M. Sharma, A. Chauhan, R. P. Singh, and T. Wagner (2011), Estimation of $NO_x$ emissions from Delhi using Car MAX-DOAS observations and comparison with OMI satellite data, *Atmos. Chem. Phys.*, *11*(21), 10,871–10,887, doi:10.5194/acp-11-10871-2011.

Stutz, J., O. Pikelnaya, G. Mount, E. Spinei, S. C. Herndon, E. C. Wood, O. Oluwole, W. Vizuette, and E. Causo (2011), Quantification of Hydrocarbon, $NO_X$, and $SO_2$ Emissions from Petrochemical Facilities in Houston: Interpretation of the 2009 FLAIR Dataset, *Rep*. *10-045*, Air Quality Research Program, University of Texas at Austin.

Svensson, F., A. Hasselrot, and J. Moldanova (2004), Reduced environmental impact by lowered cruise altitude for liquid hydrogen-fuelled aircraft, *Aerosp. Sci. Technol.*, *8*(4), 307–320, doi:10.1016/j.ast.2004.02.004.

Tucker, S. C., W. A. Brewer, R. M. Banta, C. J. Senff, S. P. Sandberg, D. C. Law, A. M. Weickmann, and R. M. Hardesty (2009), Doppler lidar estimation of mixing height using turbulence, shear, and aerosol profiles, *J. Atmos. Oceanic Technol.*, *26*(4), 673–688, doi:10.1175/2008JTECHA1157.1.

Vandaele, A. C., C. Hermans, P. C. Simon, M. Carleer, R. Colin, S. Fally, M. F. Mérienne, A. Jenouvrier, and B. Coquart (1998), Measurements of the $NO^2$ absorption cross-section from 42,000 $cm^{-1}$ to 10,000 $cm^{-1}$ (238-1000 nm) at 220 K and 294 K, *J. Quant. Spectros. Radiat. Transfer*, *59*(3-5), 171–184.

Wagner, T., O. Ibrahim, R. Shaiganfar, and U. Platt (2010), Mobile MAX-DOAS observations of tropospheric trace gases, *Atmos. Meas. Tech.*, *3*(1), 129–140, doi:10.1029/2007JD008808.

Washenfelder, R. A., et al. (2010), Characterization of NOx, $SO_2$, ethene, and propene from industrial emission sources in Houston, Texas, *J. Geophys. Res.*, *115*, D16311, doi:10.1029/2009JD013645.

Wert, B. P., et al. (2003), Signatures of terminal alkene oxidation in airborne formaldehyde measurements during TexAQS 2000, *J. Geophys. Res.*, *108*(3), 4104, doi:10.1029/2002JD002502.

Wood, E. C., et al. (2012), Combustion and destruction/removal efficiencies of in-use chemical flares in the greater Houston area, *Ind. Eng. Chem. Res.*, *51*(39), 12,685–12,696, doi:10.1021/ie202717m.